Supporting Information

Polyurethane Elastomers Based on Triple Reversible Networks with Acceleration Self-Healing by Photothermal Conversion

*Jiale Li[#], Ang Li[#], Haijiang Zhang, Jinmeng Zhang, Jiahao Chu, Yi -Xian Wu**

State Key Laboratory of Chemical Resource Engineering,

Beijing University of Chemical Technology No. 15

Beisanhuan East Road, Chaoyang District, Beijing, 100029, China

#: Jiale Li and Ang Li contributed equally to this work.

*Corresponding Author: wuyx@mail.buct.edu.cn

1. Experimental Section

Materials. Polytetramethylene ether glycol ($PTMG_{2000}$, M_n = 2000 g/mol, 99%), dicyclohexylmethane-4,4'-diisocyanate (HMDI, 99%), α-acetyl-γ-butyrolactone (99%), guanidine carbonate (99%), and triethylamine (99%) were all sourced from Macklin Biochemical Co., Ltd. Dibutyltin dilaurate (DBTDL, 95%), N,N-dimethylformamide (Extra Dry, ≥ 99%), deuterated dimethyl sulfoxide (DMSO-d_6, 99.8%), and 1,4-benzoquinone dioxime (BQDO, 99%) were procured from Aladdin Industrial Co., Ltd. Each of these reagents was used as received without further purification unless otherwise stated.

Synthesis of UPy Molecules. The functionalized UPy chain extender was synthesized as follows: Guanidine carbonate and α-acetyl-γ-butyrolactone were added to a three-neck flask containing anhydrous ethanol, which was then placed in an oil bath at 80 °C under continuous stirring. An appropriate amount of triethylamine (TEA) was introduced to initiate the reflux reaction. As the reaction proceeded, the suspension in the flask gradually turned yellow. After 12 hours of reflux, the reaction was terminated. The suspension was subjected to vacuum filtration and washed three times with anhydrous ethanol to obtain a white solid powder. This powder was then dispersed in deionized water under high-speed stirring, and the pH of the suspension was adjusted to 6–7 using a 0.1 mol/L dilute hydrochloric acid solution. Following another vacuum filtration step, the resulting white filter cake was washed again with anhydrous ethanol to achieve efficient purification of the functionalized small molecules. The purified product was vacuum-dried in an oven at 60°C for 24 hours, yielding a white powder identified as the functionalized UPy chain extender. The synthetic route is illustrated in Scheme S1.

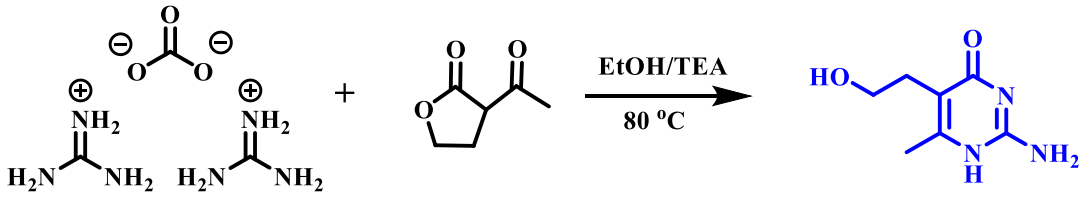

Scheme S1 Synthesis route of functionalized UPy chain extender.

Pre-polymerization of OCN-PTMG-NCO prepolymers. A series of photothermal polyurethanes with synergistic self-healing properties through dynamic oxime bonds and hydrogen bonding were

synthesized using functionalized UPy and 1,4-benzoquinone dioxime (BQDO) as chain extenders at varying molar ratios. The synthetic procedure was carried out as follows: First, 5 g of $PTMG_{2000}$ was charged into a three-neck flask and dehydrated under vacuum at 120 °C for 2 h to minimize residual moisture. After dehydration, the flask was placed in an oil bath equipped with magnetic stirring at 60 °C. Under a nitrogen atmosphere, 1.34 g of HMDI and 3 mg of DBTDL were introduced. The reaction temperature was gradually raised from 60 °C to 80 °C and maintained for 4 h, yielding an isocyanate-terminated polyurethane prepolymer.

Synthesis of TPU-BU Polymer. Subsequently, the temperature of the prepolymer was lowered to 60 °C. The two-component chain extender system—including UPy and BQDO—was dissolved in 20 mL of DMF according to the calculated formulation in **Table S1** and then added to the prepolymer after complete dissolution. (Typically, 20 mL dehydrated DMF solution with 0.17 g of BQDO and 0.21 g of UPy was added into the prepolymerization solution for TPU-$B_{50}U_{50}$) Following homogeneous mixing, the temperature was carefully increased from 60 °C to 80 °C to avoid rapid polymerization. The reaction was continued under nitrogen for another 4 h. During this period, samples were periodically taken for FTIR analysis to monitor the decrease in absorption intensity of the isocyanate characteristic peak at 2320 cm^{-1}. The reaction was considered complete when this peak disappeared, at which point the mixture was ready for film casting. The final polyurethane solution was poured into a square polytetrafluoroethylene mold and dried in a forced-air oven at 80 °C for three days, affording an elastomeric film exhibiting self-healing behavior enabled by the cooperation of dynamic oxime-carbamate bonds and hydrogen bonds.

2. Characterizations

FTIR analysis. The samples were characterized by Fourier transform infrared (FTIR) spectroscopy and variable-temperature FTIR using a Nicolet 6700 spectrometer (Thermo Fisher Scientific, USA) over a wavenumber range of 4000–400 cm^{-1}, with 32 scans and a resolution of 4 cm^{-1}. The conversion of resulting polymers was calculated based on absorbance at 2350, 1699 and 1635 cm^{-1} assigned to NCO, BQDO and UPy, respectively, as shown in **Equation S1**.

$$conv_{NCO} = \left(1 - \frac{A_{r,2350}}{A_{0,2350}}\right) \times 100\% \quad \text{eq.(S1-1)}$$

$$conv_{BQDO} = \left(1 - \frac{A_{r,1699}}{A_{0,1699}}\right) \times 100\% \quad \text{eq.(S1-2)}$$

$$conv_{UPy} = \left(1 - \frac{A_{r,1635}}{A_{0,1635}}\right) \times 100\% \quad \text{eq.(S1-3)}$$

Where $conv_{NCO}$, $conv_{BQDO}$ and $conv_{UPy}$ indicate the conversion based on absorbance of NCO, BQDO and UPy, respectively. A_r and A_0 indicate the absorbance of resulting product and original reactant, respectively.

The FTIR spectra in the range of 1800–1500 cm^{-1} were analyzed by *Gaussian Fitting* according to our previous report.[8]

^{1}H NMR characterization. Proton nuclear magnetic resonance (^{1}H NMR) spectrum of chain extender was recorded on an AV400 MHz NMR spectrometer (Bruker, Germany) in deuterated dimethyl sulfoxide (DMSO-d_6).

UV-vis analysis. UV–visible spectra were collected in the range of 200-1000 nm at a resolution of 1 nm by using a PERSEE T700 UV–vis spectrophotometer (Beijing Puxi, China), with background subtraction applied, according to our previous report.[26]

X-ray diffraction analysis. X-ray diffraction (XRD) analysis was performed on a D8 ADVANCE diffractometer (Bruker, Germany) with CuKα radiation (λ = 0.154 nm). Data were collected in the 2θ range of 10–90° at 25°C with a scanning rate of 5 °/min. The interplanar spacing (*d*) and the angle (θ) between the incident X-ray and the corresponding crystal plane follow Bragg's Law (**Equation S2**).

$$2\,d\,sin\,\theta = n\lambda \quad \text{eq.(S2)}$$

TEM observation. The phase-separated structure of the material was observed *via* a Hitachi HT-7700 transmission electron microscope after staining with osmium tetroxide. The sample was prepared as a 1 mg/mL solution in DMF, dropped onto a bare copper grid, and annealed at 60°C for 24 h.

SEM observation. The surface and cross-sectional microstructures of swollen samples were examined using an S-4700 scanning electron microscope (Hitachi, Japan) under an accelerating voltage of 20 kV and a current of 10 μA, at 25°C and 51% humidity.

DSC analysis. Thermal behavior was analyzed *via* a Q-200 differential scanning calorimeter (TA Instruments, USA), according to our previous report.[8]

Rheological tests. Rheological properties were measured on a DHR-2 rheometer (TA Instruments) with a 25 mm parallel-plate fixture and a gap of 1000 μm. Oscillation temperature sweeps were conducted from 30 to 120°C at a heating rate of 3 °C/min, with a frequency of 1 Hz and a shear strain amplitude of 0.1%. Oscillation frequency sweeps were carried out at temperatures ranging from 50 to 120 °C in 10 °C increments, over a frequency range of 0.01 to 100 Hz and at a constant strain amplitude of 0.1%. The frequency curves were fitted by *Williamson model*, accessing the zero-shear viscosity according to **Equation S3**.

$$\eta = \frac{\eta_0}{1 + (\lambda\dot{\gamma})^n} \qquad \text{eq.(S3)}$$

where η denotes the viscosity corresponding to the shear rate $\dot{\gamma}$; η_0 is the zero-shear viscosity, which is the target parameter for derivation; λ represents the relaxation time constant; n is the dimensionless power-law exponent; and $\dot{\gamma}$ signifies the shear rate. And the η_0 obeys the Arrhenius relationship with temperature T, allowing the activation energy ($E_{a,\tau}$) determined by **Equation S4.**

$$ln\,\eta = -\frac{E_{a,\eta}}{RT} + ln\,\eta_0 \qquad \text{eq.(S4)}$$

where R is the universal gas constant, T is the environmental temperature.

DMA characterization. The dynamic thermomechanical properties of TPU-BU polymer films were evaluated using a Q800 dynamic mechanical analyzer (TA Instruments, USA). Specimens were cut into rectangular strips with the dimensions of 5 × 25 × 0.5 mm³. Temperature sweeps were performed in tensile film mode from –100 to 100°C at 3 °C/min, with a amplitude of 0.1% and a

frequency of 1 Hz. Stress relaxation tests were conducted under the same fixture at constant temperatures of 50~80 °C. A tensile strain of 5% was applied, and the stress was recorded for 40 minutes. Data were processed using TA Trios software to obtain normalized stress relaxation modulus curves, from which the characteristic relaxation time (τ) at 1/e was derived. The relaxation time (τ) obeys the Arrhenius relationship with temperature T, allowing the activation energy ($E_{a,\tau}$) to be determined using **Equation S5.**

$$ln\,\tau = -\frac{E_{a,\tau}}{RT} + ln\,\tau_0 \qquad \text{eq.(S5)}$$

where R is the universal gas constant, T is the absolute temperature, and τ_0 is the relaxation time at infinite temperature.

Photothermal conversion. The photothermal conversion mechanism was investigated *via* UV–vis spectroscopy for BQDO monomer, TPU-BU polymer solutions, and elastomer films over 200–1000 nm, according to reference.[26] The monomer and polymer solutions were prepared in DMF at 1 mg/mL, while the elastomer film was measured against an air background. An 808 nm near-infrared laser module was used as the light source, and surface temperature changes were recorded with a Hikvision K20 thermal imager. Specific test procedures were as follows:

(1) TPU-BU polymer elastomer films were cut into 1 × 1 cm² squares and irradiated with NIR lasers at 200 mW·cm^{-2} and 500 mW·cm^{-2}, with a vertical distance of 10 cm between the laser and the sample. The laser was turned off once the surface temperature stabilized, and natural cooling was monitored. The entire process was recorded by the thermal imager.

(2) The photothermal conversion efficiency and thermal conductivity were calculated according to **Equation (S6)** in the literature.

$$\frac{\Delta Q}{\Delta t} = -\lambda\left(\frac{dT}{dx}\right)_{x_0} \times S_{in} = \lambda\frac{T_0 - T_1}{h_1}S_{in} \qquad \text{eq. (S6-1)}$$

$$\frac{\Delta Q}{\Delta T} = mc\left(\frac{\Delta T}{\Delta t}\right)_{T=T_0} \times S_{dis} \qquad \text{eq. (S6-2)}$$

$$\mathrm{PCE} = \frac{P_{dis}}{P_{in}} = \frac{\lambda S_{in}(T_0 - T_1)}{P_{in}h_1} \qquad \text{eq. (S6-3)}$$

The S_{in}, S_{dis}, I_{808} and I_{dis} indicate the areas and powers of energy input or heat dissipation process respectively. The m, c and h_1 indicate the weight, specific heat and height of polymer films respectively.

(3) Photothermal cycling tests were conducted under similar conditions: the elastomer film was irradiated for 60 s, followed by 60 s of cooling, constituting one cycle. Four consecutive heating–cooling cycles were performed without interruption, with temperature changes recorded throughout.

Mechanical properties and cyclic tensile tests of TPU-BU polymer were performed on an Instron 3345 universal testing system (USA). The self-healing efficiency is determined based on cyclic tensile tests through the calculation of the dissipated energy per cycle and the application of **Equation (S7)**.

$$\eta(X) = \frac{H(X)}{H_0} \qquad \text{eq. (S7-1)}$$

$$\eta(x) = e^{bx/t} \qquad \text{eq. (S7-2)}$$

$$\lim_{x\to\infty} \eta(x) = \eta_d \qquad \text{eq. (S7-3)}$$

DFT Analysis. Both the geometry optimization and the frequency calculations were performed with the Gaussian 09 program package and run at the D3-corrected levels of B3LYP functional with an ultrafine grid.[26] The hybrid density functional B3LYP was used in intense investigation and showed excellent performance for providing the conformation of the vanadium complexes. A treble -ζ-quality basis set 6- 311G(d,p) was used for C, H, O and S atoms and a SDD basis set was used for Fe atom. Based on the optimized geometries, the frequency analysis was also performed and no imaginary frequency was discovered.

Self-healing tests. For self-healing rheology tests, amplitude sweeps (0.01–1000%) were performed at a fixed frequency of 1 Hz. Subsequently, a five-cycle step-strain test was carried out: each cycle consisted of 60 s at 0.01% strain (low-strain region) followed by 60 s at a high strain (determined from amplitude sweep results), with a 5-minute recovery interval between cycles. The self-healing efficiency can be evaluated by comparing the changes in storage modulus and loss modulus using **Equation (S8)**.

$$\eta_E = \frac{G'}{G_0'} \times 100\% \qquad \text{eq. (S8-1)}$$

$$\eta_v = \frac{G''}{G_0''} \times 100\% \qquad \text{eq. (S8-2)}$$

where η_E denotes the recovery efficiency of the storage modulus; η_v denotes the recovery efficiency of the loss modulus; G' represents the storage modulus; and G'' represents the loss modulus.

The self-healing efficiency of PTA-Fe specimen was evaluated by fracture tensile test. The PTA-Fe films mentioned above were cut into two species and the cracked surfaces were fixed. After healing under various conditions for various duration, the healed specimen was performed on universal mechanical test for three times, according to the method mentioned above. The self-healing efficiency based on stress could be calculated according to **Equation (S8)**.

$$\eta_T = \frac{\sigma_{T,heal}}{\sigma_{T,0}} \times 100\% \qquad \text{eq. (S9)}$$

3. Supplementary Tables

Table S1 Raw materials feeding ratios and chemical compositions of TPU-BU polymers

Samples	$PTMG_{2000}$/mmol	HMDI/mmol	BQDO/mmol	UPy/mmol
$TPU\text{-}B_{100}U_0$	2.5	5.1	2.5	0
$TPU\text{-}B_{75}U_{25}$	2.5	5.1	18.8	6.2
$TPU\text{-}B_{50}U_{50}$	2.5	5.1	12.5	12.5
$TPU\text{-}B_{25}U_{75}$	2.5	5.1	6.2	18.8
$TPU\text{-}B_0U_{100}$	2.5	5.1	0	2.5

4. Construction of TPU with Various Hard-Segmental Structures

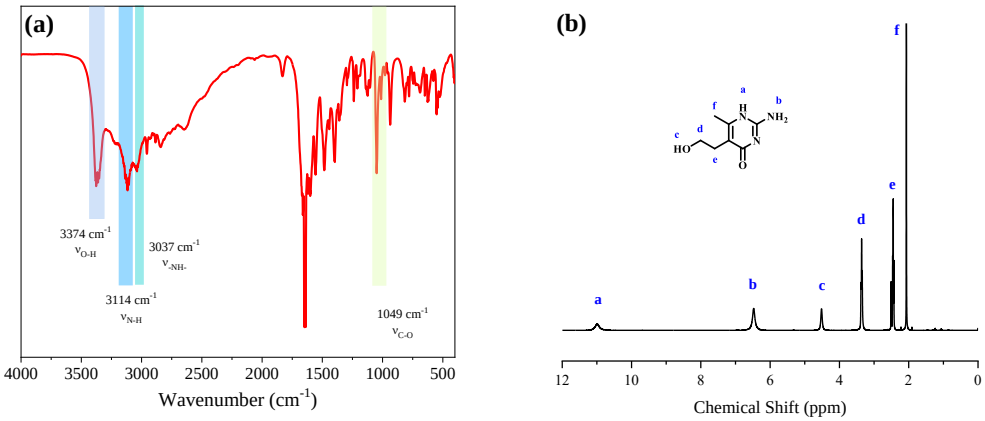

Figure S1 (a) FTIR and (b) ^{1}H-NMR spectra of UPy.

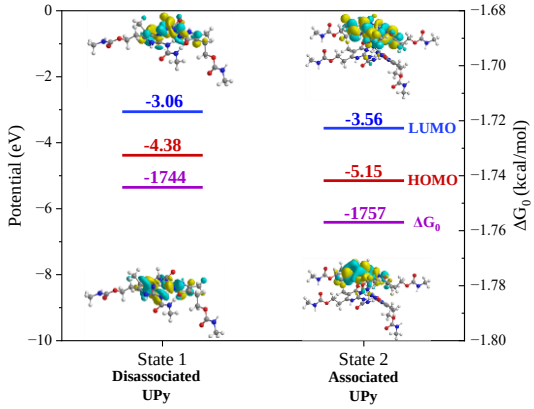

Figure S2 DFT analysis for frontier molecular orbitals and standard Gibbs free energy at 298.15 K (ΔG_0) of UPy at various states.

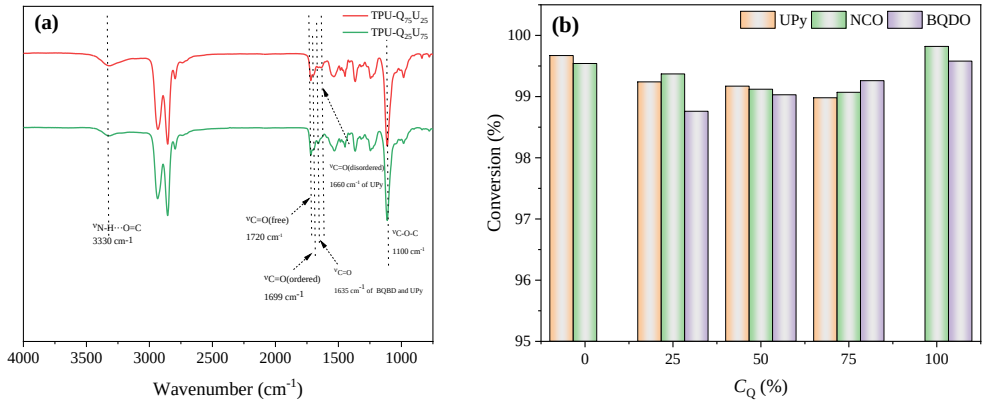

Figure S3 (a) FTIR spectra of TPU-$Q_{75}U_{25}$ and TPU-$Q_{25}U_{75}$ polymers. (b) Relationships between C_Q and conversion of resulting polymers calculated based on FTIR spectra.

5. Supramolecular Networks Based on Interactions in Hard Segments of TPU.

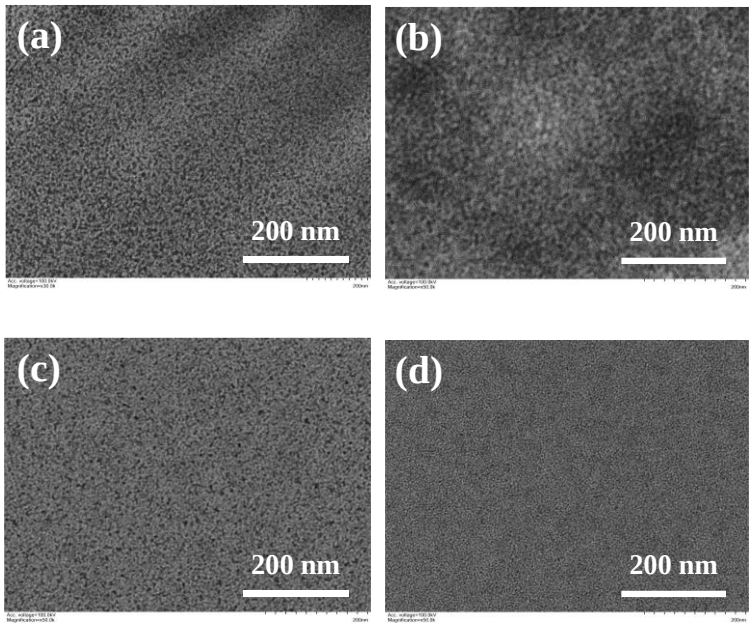

Figure S4 TEM images of (a) TPU-Q, (b) TPU-$Q_{50}U_{50}$, (b) TPU-$Q_{25}U_{75}$ and (c) TPU-U.

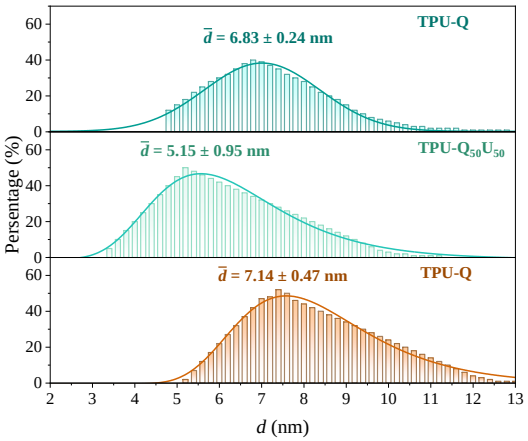

Figure S5 Statistical histograms of hard-segmental sizes according to **Figure S4**.

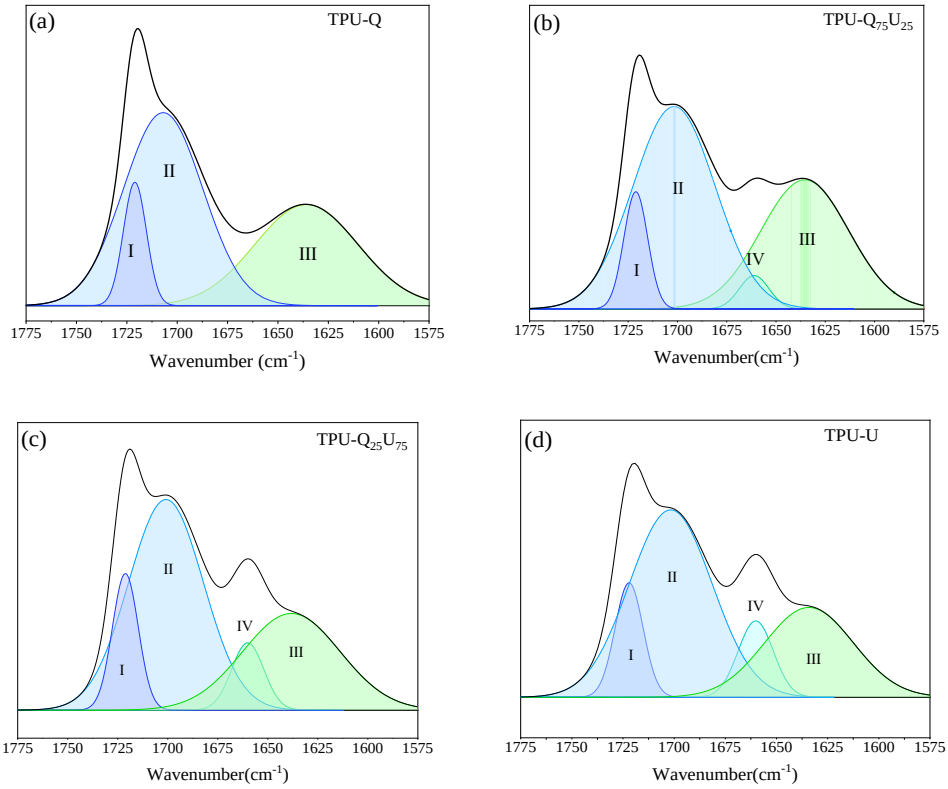

Figure S6 *Gauss* fitting result of FTIR spectra of (a) TPU-Q, (b) TPU-$Q_{75}U_{25}$, (c) TPU-$Q_{25}U_{75}$, and (d) TPU-U polymers in wavelength range of 1775~1575 cm^{-1}.

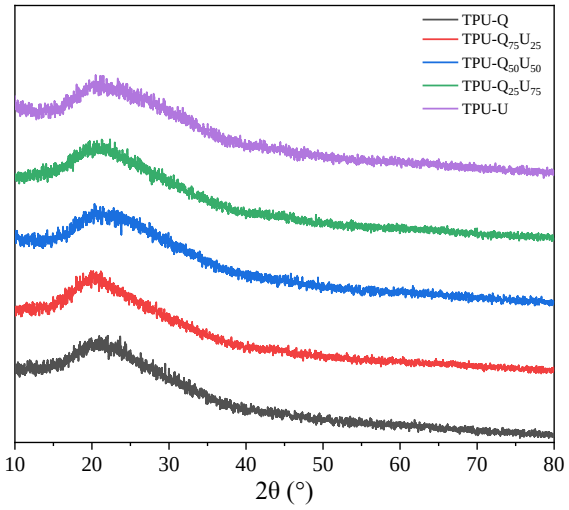

Figure S7 XRD patterns of TPU-QU polymers.

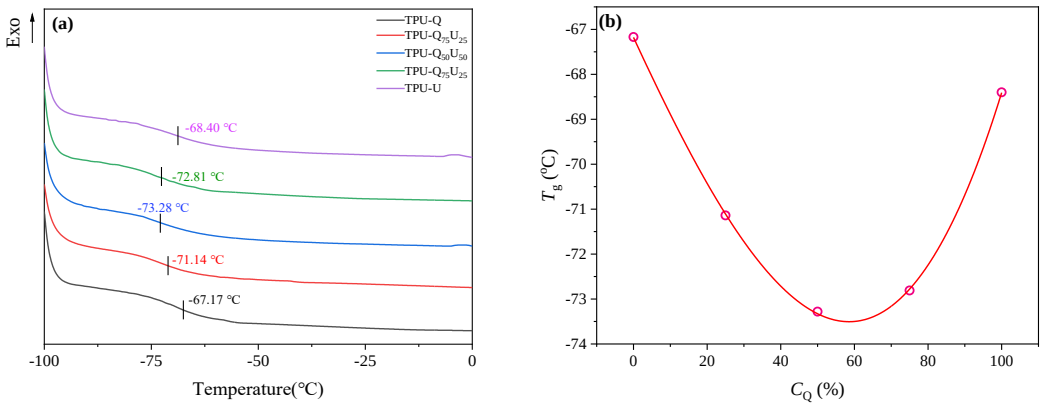

Figure S8 (a) DSC curves of TPU-QU polymers and (b) corresponding relationship between T_g and C_Q.

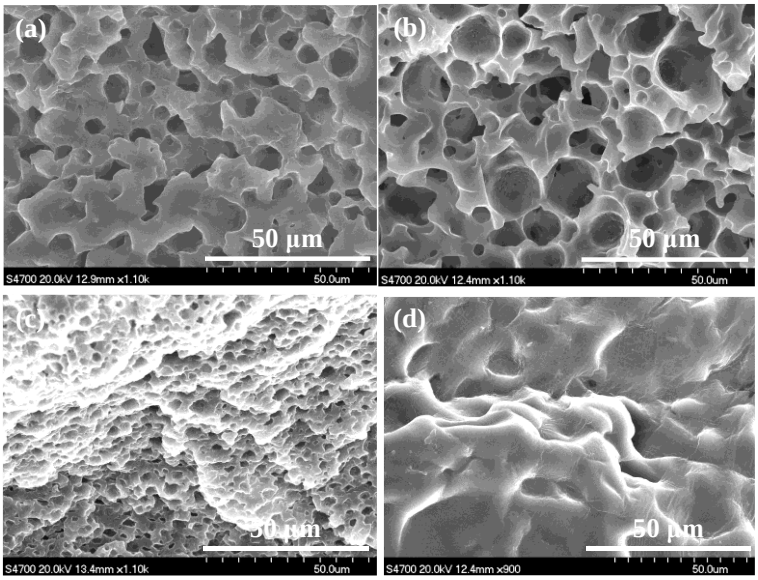

Figure S9 SEM image for cross-sectional micromorphology of frozen-dried (a) TPU-U, (b) TPU-$Q_{25}U_{75}$, (c) TPU-$Q_{75}U_{25}$ (a) TPU-Q after swollen in DMSO for a week.

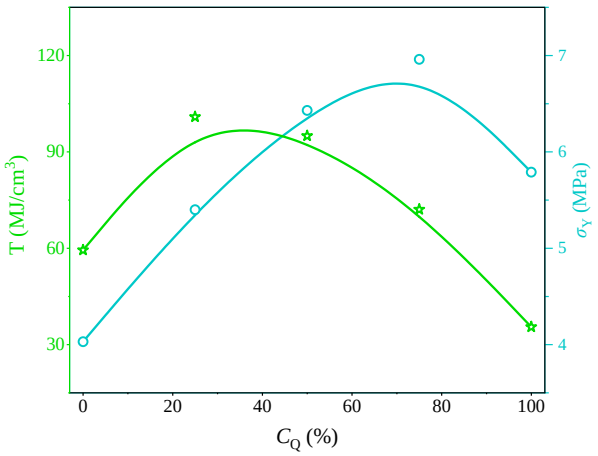

Figure S10 Relationships between toughness (T) or and Young's modulus (σ_Y) and C_Q.

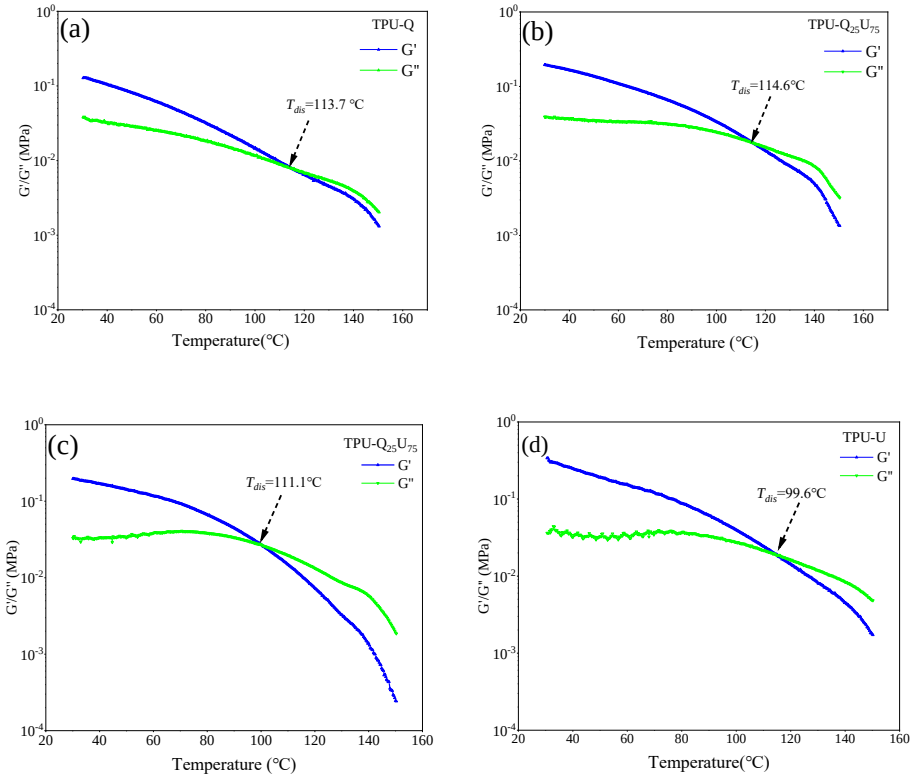

Figure S11 Oscillation temperature ramp of (a) TPU-Q, (b) TPU-$Q_{75}U_{25}$, (c) TPU-$Q_{25}U_{75}$, and (d) TPU-U.

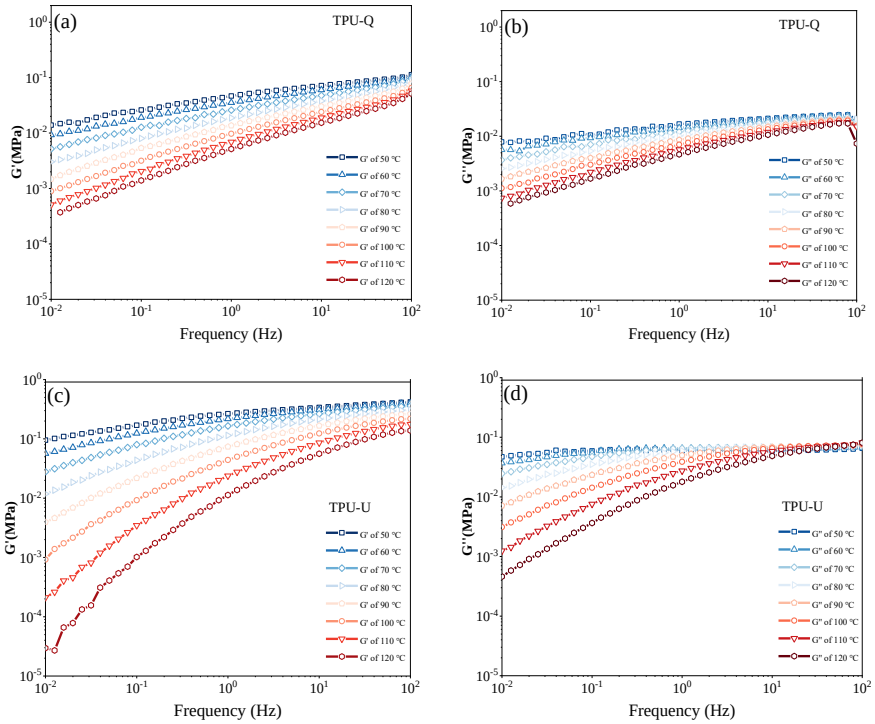

Figure S12 (a, c) G’ curves and (b, d) G’’ curves of TPU-Q and TPU-U respectively at various temperature.

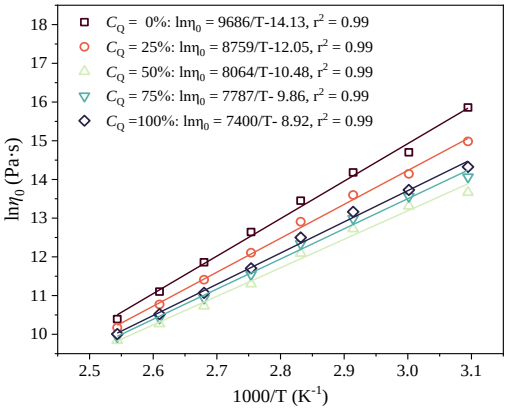

Figure S13 Linear relationship between lnη_0 and 1000/T according to frequency ramp.

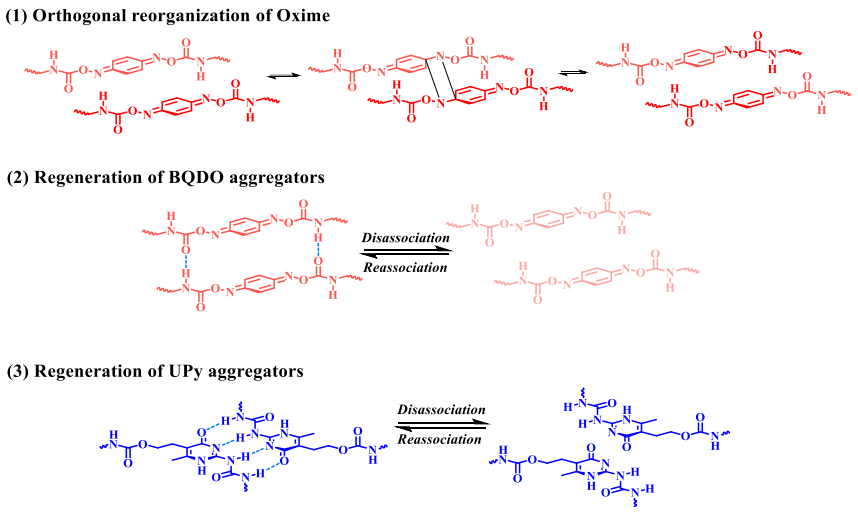

Scheme S2 *Possible mechanism of the thermal reversible process for TPU-QU.*

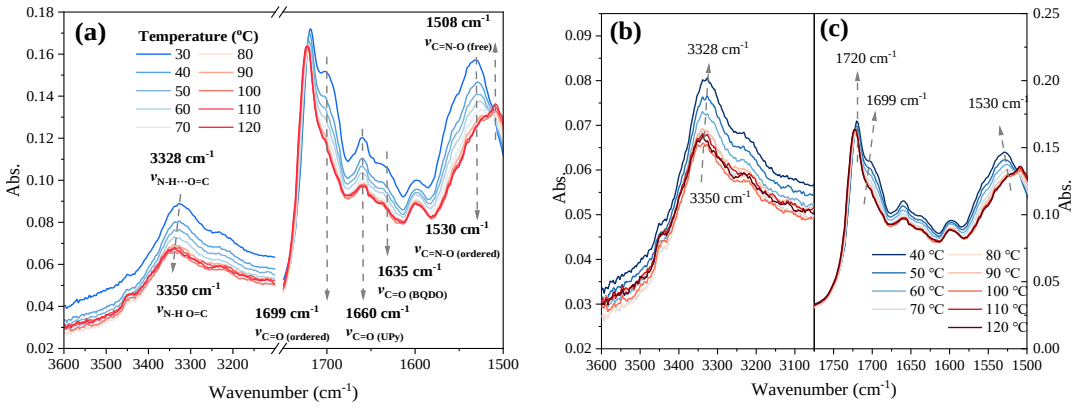

Figure S14 VT-FTIR spectra of TPU-$Q_{50}U_{50}$ supramolecular networks during (a) heating process with the rate of 5 °C/min and (b, c) natural cooling process.

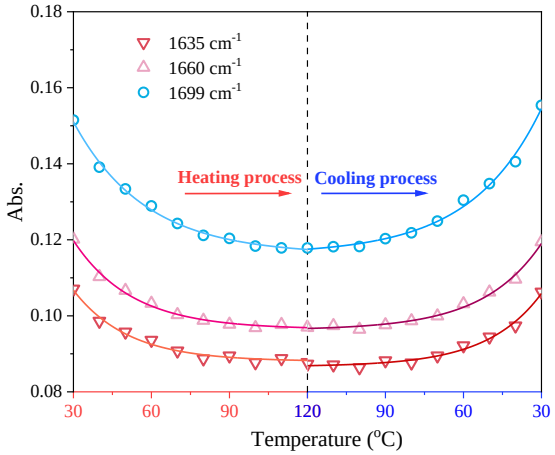

Figure S15 Relationship between temperature and absorbance at 1699, 1660 or 1635 cm^{-1} according to **Figure S14**.

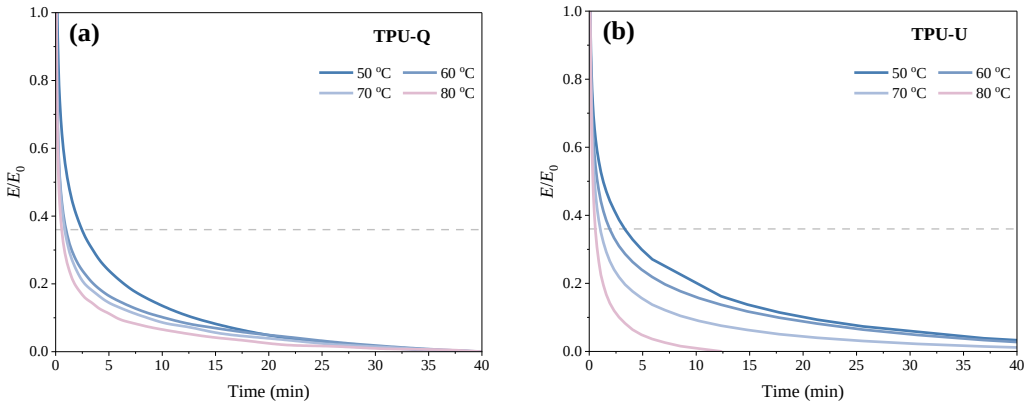

Figure S16 Stress-relaxation curves of (a) TPU-Q and (b) TPU-U at various temperature.

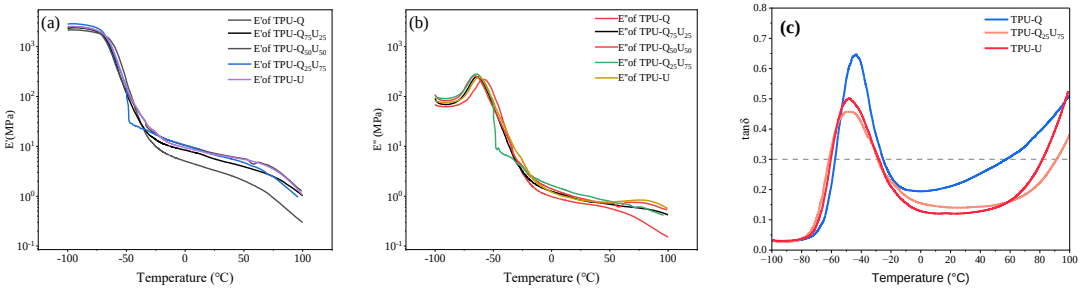

Figure S17 (a) Storage modulus, (b) loss modulus and (c) tanδ of TPU-QU at various temperature.

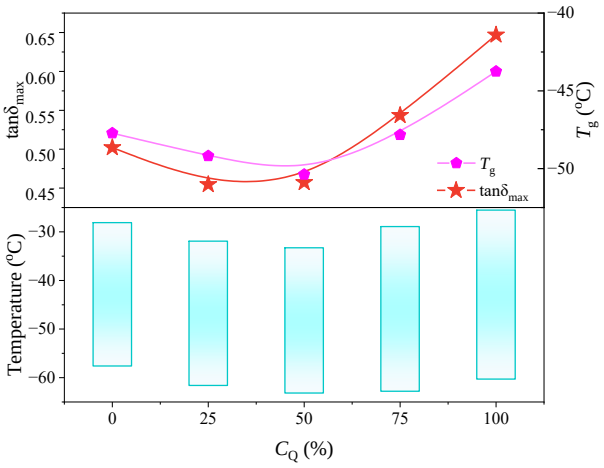

Figure S18 Effect of C_Q on damping range, $\tan\delta_{max}$ and T_g.

6. Rapid Self-healing of TPU Promoted by Photothermal Conversion.

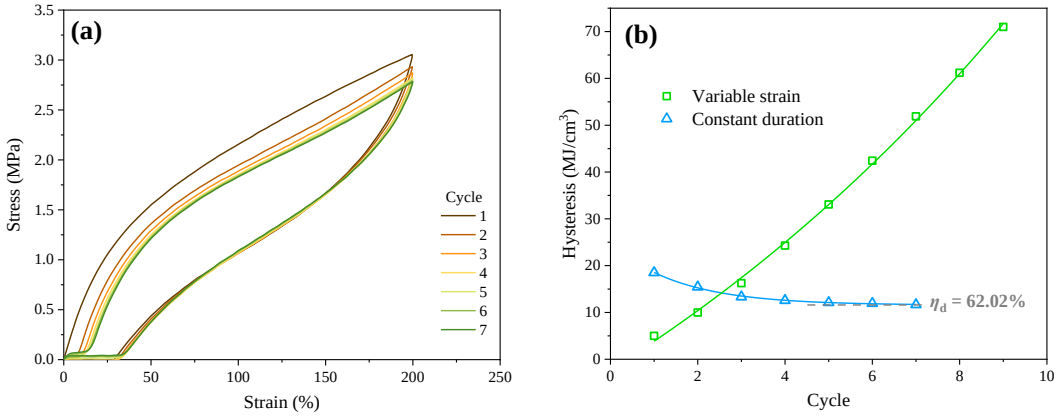

Figure S19 (a) Cyclic stress-strain curves of TPU-$Q_{50}U_{50}$ specimens by setting self-healing duration. (b) Relationships between hysteresis and cycle number according to (a).

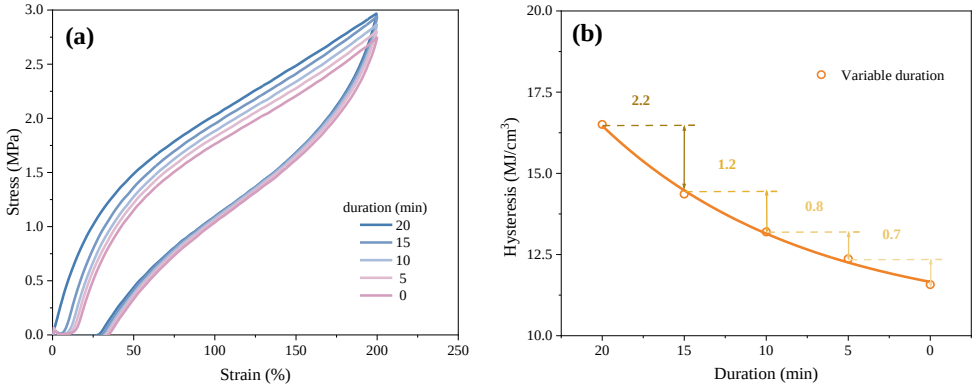

Figure S20 Cyclic stress-strain curves of TPU-$Q_{50}U_{50}$ specimens by varying self-healing duration. (b) Relationships between hysteresis and self-healing duration according to (a).

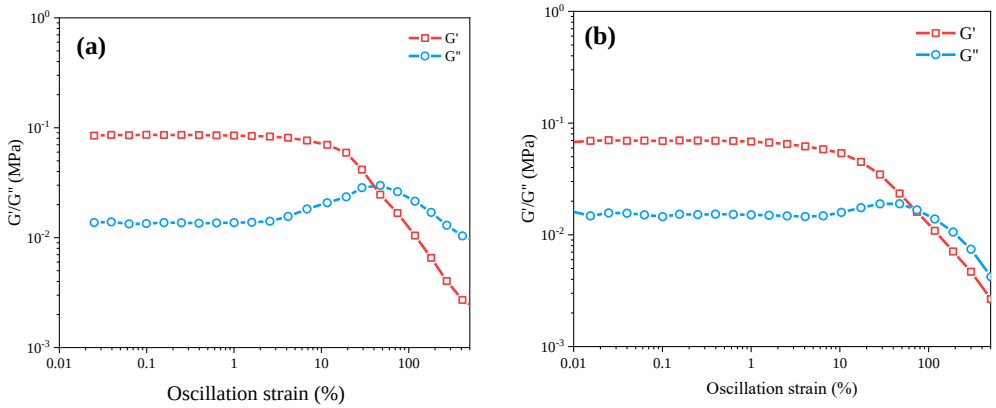

Figure S21 Oscillation shearing ramp of (a) TPU-$Q_{50}U_{50}$ and (b) TPU-$Q_{75}U_{25}$ (f = 1 Hz, T = 80 °C).

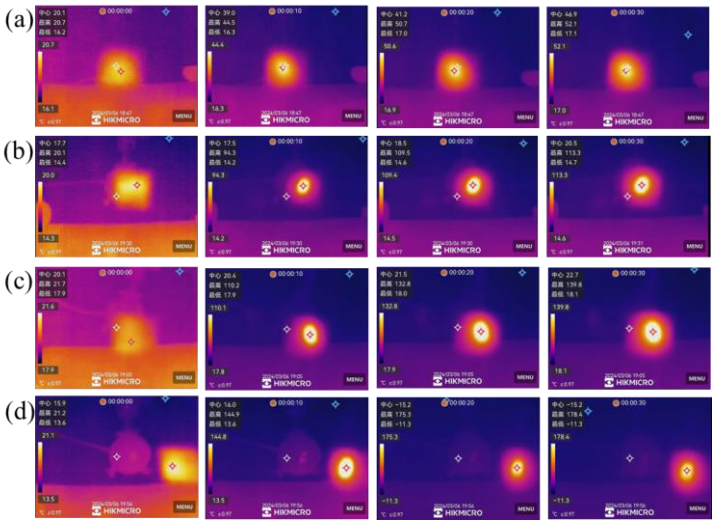

Figure S22 Infrared images of (a)TPU-$Q_{25}U_{75}$, (b)TPU-$Q_{50}U_{50}$, (c)TPU-$Q_{75}U_{25}$, and (d)TPU-Q film under NIR irradiation (200 mW·cm^{-2}) at various time.

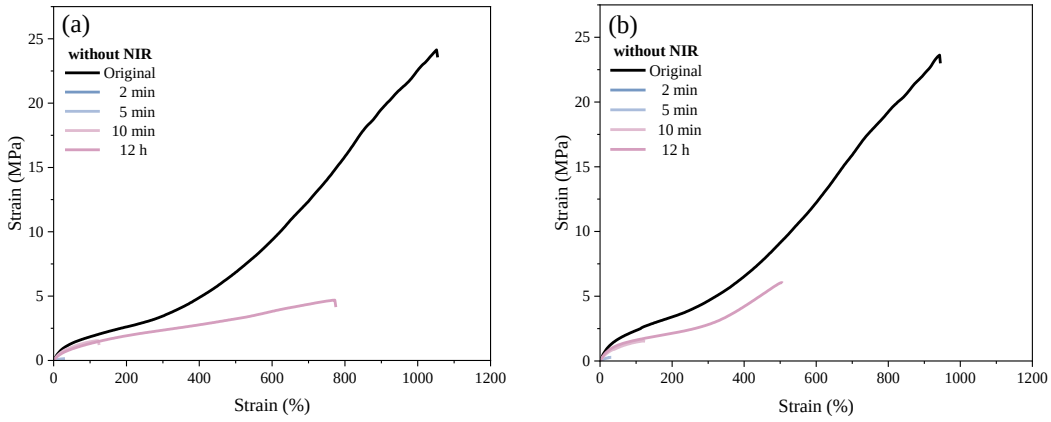

Figure S23 Stress-strain curves of (a) TPU-$Q_{75}U_{25}$ and (b) TPU-$Q_{50}U_{50}$ specimens at original state and self-healing without NIR irradiation for various duration.

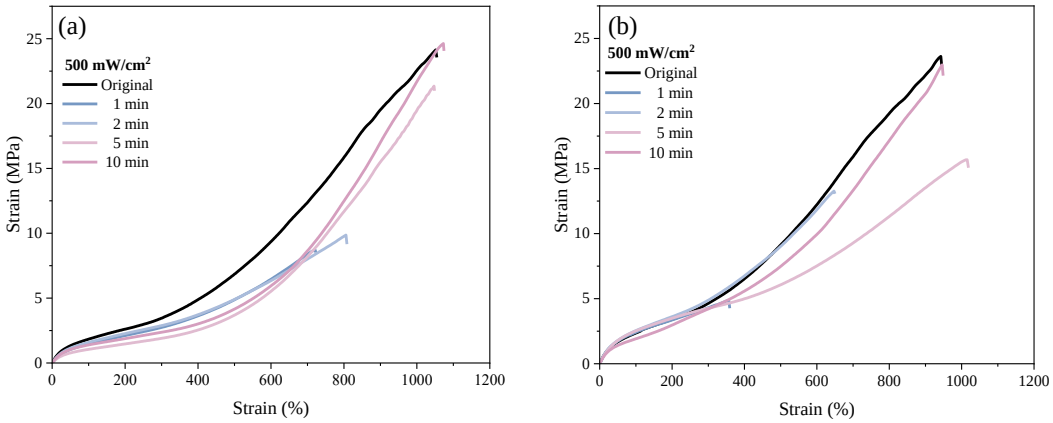

Figure S24 Stress-strain curves of (a) original TPU-$Q_{75}U_{25}$ specimens and that after self-healing under NIR irradiation (I_{808} = 500 mW·cm^{-2}) for various duration; (b) original TPU-$Q_{50}U_{50}$ specimens and that after self-healing under NIR irradiation (I_{808} = 500 mW·cm^{-2}) for various duration.

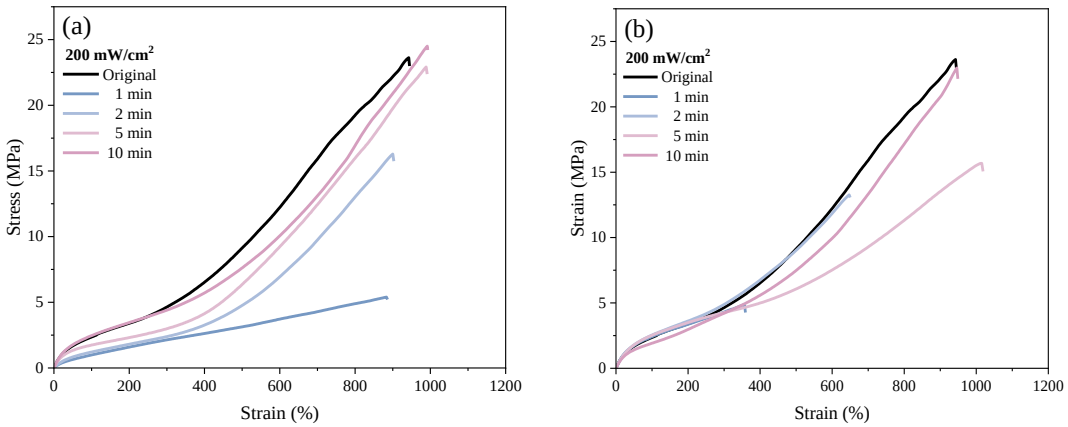

Figure S25 Stress-strain curves of (a) original TPU-$Q_{75}U_{25}$ specimens and that after self-healing under NIR irradiation (I_{808} = 200 mW·cm^{-2}) for various duration; (b) original TPU-$Q_{50}U_{50}$ specimens and that after self-healing under NIR irradiation (I_{808} = 200 mW·cm^{-2}) for various duration.

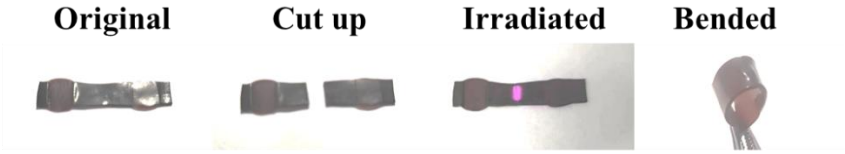

Figure S26 The self- self-healing process of TPU-$Q_{75}U_{25}$ specimens under NIR irradiation at I_{808} of 200 mW·cm^{-2} within 10 min.

Figure S27 TPU-$Q_{75}U_{25}$ specimen loaded weight of 2.5 kg after self- self-healing under NIR irradiation at I_{808} of 200 mW·cm^{-2} within 10 min.

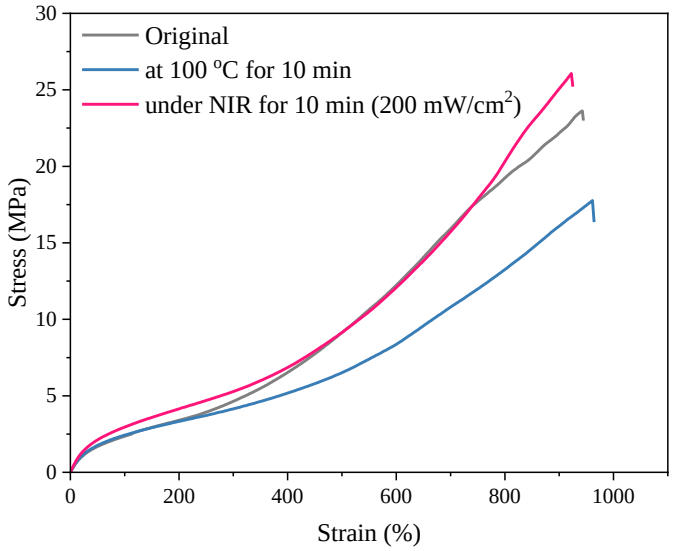

Figure S28 Stress-strain curves of original TPU-$Q_{75}U_{25}$ specimens and that after self-healing under NIR irradiation (I_{808} = 200 mW·cm^{-2}) or heating at 100 °C for 10 min.

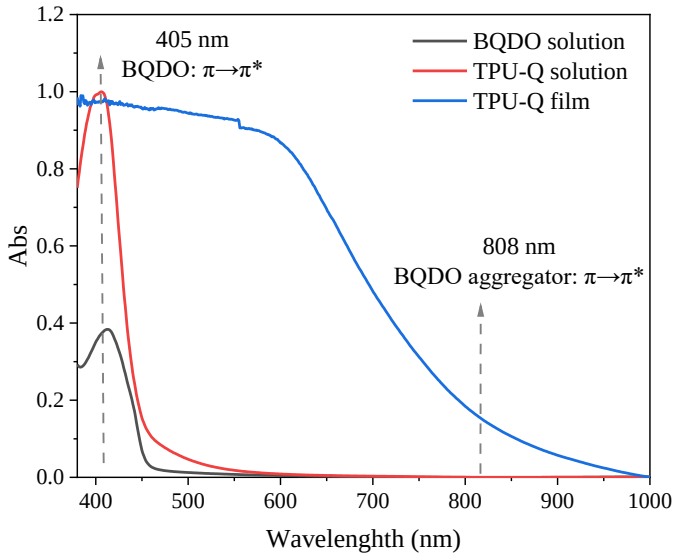

Figure S29 Vis-NIR spectra of TPU-Q and BQDO at different states.